

Non-dispersive solvent extraction of *p*-toluic acid from purified terephthalic acid plant wastewater with *p*-xylene as extractant^{*}

Qing-ran KONG, You-wei CHENG, Li-jun WANG, Xi LI^{†‡}

(College of Chemical and Biological Engineering, Zhejiang University, Hangzhou 310027, China)

[†]E-mail: lixi@zju.edu.cn

Received Oct. 23, 2015; Revision accepted Mar. 5, 2016; Crosschecked Sept. 23, 2016

Abstract: Non-dispersive solvent extraction (NDSE) with *p*-xylene as extractant was employed as a novel separation method to recover both *p*-toluic (PT) acid and water from purified terephthalic acid (PTA) wastewater. The mass transport behavior of PT acid from aqueous solution to *p*-xylene was investigated by experiments and numerical simulation. Experiments showed that NDSE is feasible and effective. Residual PT acid in the raffinate can be reduced to lower than the permitted limit of wastewater re-use (100 g/m³) with extraction time longer than 60 s in industrial conditions. A mathematical model of PT acid mass transport was developed to optimize the membrane module performance. The model was validated with the experimental results with relative errors of less than 6%. Numerical analysis for mass transfer through the lumen side, the porous membrane layer, and the shell side showed that PT acid transport in the aqueous solution is the rate determining step. The effects of the membrane and operating parameters on membrane module performance were investigated by means of computational simulations. The key parameters suggested for industrial NDSE design are: fiber inner radius $r_1=200\text{--}250\ \mu\text{m}$, extraction time $t_e=50\text{--}60\ \text{s}$, aqueous/organic volumetric ratio $a/o=9.0$, and temperature $T=318\ \text{K}$.

Key words: Non-dispersive solvent extraction (NDSE), Purified terephthalic acid (PTA) wastewater, *p*-toluic (PT) acid, *p*-xylene (PX), Mass transfer

<http://dx.doi.org/10.1631/jzus.A1500281>

CLC number: TQ09

1 Introduction

Purified terephthalic acid (PTA) is a feedstock of the polyester industry. Global production of PTA was more than 50 million tons in 2014 (Sun, 2014). As a result, a huge amount of wastewater is discharged following the hydrogenation step of the PTA process. PTA wastewater contains mostly *p*-toluic (PT) acid, which is generated by the catalytic hydrogenation of the key impurity, 4-carboxybenzaldehyde (Li *et al.*, 2014). Evidence indicates that aromatic acids have serious side ef-

fects on environmental protection and human health, thus, the direct discharge of PTA wastewater into natural waterways is strictly forbidden (Macarie *et al.*, 1992; Daramola *et al.*, 2011). At present, PTA wastewater is treated mostly by anaerobic biological methods to degrade the aromatic acid (Kleerebezem *et al.*, 2005) before discharge. The bio-treatment has a low degradation efficiency for aromatic acids (Thiruvenkatachari *et al.*, 2007), and the wastewater treatment is costly and troublesome (Liu and Cheng, 2014). About 1.5–2.0 t of wastewater, which originally comes from deionized water, has to be discharged to produce 1 t of PTA. Therefore, a more resource-saving and cost effective method is urgently required for PTA wastewater treatment.

In recent years a novel extraction method using *p*-xylene (PX) as the extractant for recovering PT acid and water from PTA wastewater has been

[‡] Corresponding author

^{*} Project supported by the National Natural Science Foundation of China (No. 20806072)

 ORCID: Qing-ran KONG, <http://orcid.org/0000-0002-0749-9161>; Xi LI, <http://orcid.org/0000-0002-4866-5672>

© Zhejiang University and Springer-Verlag Berlin Heidelberg 2016

proposed (Nakao *et al.*, 2006; Wang *et al.*, 2014). PT acid originates as an intermediate of PX oxidation to PTA, and is therefore easy to extract using PX. The extractant rich in PT acid after extraction is fed back directly to the oxidation step of the PTA process without separation of solute and solvent. In this way PT acid, together with PX, converts into PTA product. This method is cost effective and most of the PT acid in wastewater can be recovered. Nevertheless, the recommended apparatus, i.e., an extraction column (Wang *et al.*, 2014) and mixer-settler (Nakao *et al.*, 2006), will inevitably cause the emulsification of solvents and entrainment by water, which leads to secondary pollution in water requiring further purification (Zhu *et al.*, 2015). This situation is more serious for PTA wastewater treatment, because the initial concentration of PT acid in water is quite low (500–900 g/m³), so a very small amount of emulsion entrainment is intolerable.

Non-dispersive solvent extraction (NDSE) is therefore the best choice for the extraction of PTA wastewater. The structure of an NDSE module is similar to that of a tube-shell heat exchanger, which contains thousands of hollow fibers. Water and solvent flow separately through the tube and shell side, and contact each other at the porous walls of the hollow fibers. NDSE is a continuous phase extraction without dispersion and subsequent emulsification. The water raffinate treated by NDSE contains little PT acid but no PX emulsion. It is expected that the aqueous solution with a PT acid content of less than 100 g/m³ can be recycled in the hydrogenation step of the PTA process as fresh solvent solution (Li *et al.*, 2010), so most water raffinate from NDSE can be re-used. Thus, the simplest liquid-liquid extraction configuration is sufficient for purifying the PTA wastewater, and the PT acid does not need to be recovered from the extractant after NDSE. With the advantages of no emulsification and high extraction efficiency (Pabby and Sastre, 2013), NDSE has been used in many applications, including the chemical separation of pesticides (Đorđević *et al.*, 2014), bisphenol A (Gupta *et al.*, 2014), toluene (Barati *et al.*, 2014), fermentation products (Shirazian and Ashrafizadeh, 2011), zinc chloride and hydrochloric acid (Lum *et al.*, 2014), 1-butanol and acetone (Moreno *et al.*, 2014), cephalixin (Hao *et al.*, 2014), Co (Vernekar *et al.*, 2013), Lu (Kumrić *et al.*, 2012), U

(Dixit *et al.*, 2013), Zn (Samaniego *et al.*, 2007), and Cu (Ren *et al.*, 2008). However, there have been no published studies of NDSE applied to PTA wastewater.

In this study, an attempt was made to develop a novel NDSE method for simultaneously recovering PT acid from wastewater and recycling the water resource, while avoiding solvent emulsification and entrainment. Firstly, experiments were carried out to evaluate the feasibility of NDSE for PTA wastewater treatment, and to investigate the impacts of operating conditions. Then, we carried out modeling and simulation of extraction of PT acid by PX in NDSE. The rate determining step was identified. The effects of the operating and membrane parameters on membrane module performance were investigated by the simulation. Finally, optimal parameters are suggested for industrial NDSE design.

2 Experiments

A lab-scale membrane module was assembled for NDSE experiments (Table 1). The housing of the membrane module was stainless steel sealed with PX resistant epoxy at each end. The polypropylene hollow fiber used was a commercial product from the Hangzhou H-Filtration Membrane Technology & Engineering Co., Ltd., China. The length of the fiber was designed to be as long as possible to ensure that the experimental NDSE performance was close to that of an industrial module (usually 1.0 m). However, large numbers of fibers were not needed in the module because the mass transport behavior is identical for each fiber. A similar design, using only a single hollow fiber, was used by Kumrić *et al.* (2012). The essential structural and physical parameters of the fiber were provided by the supplier (Table 1).

The setups of the NDSE experiments are shown in Fig. 1. The hollow fiber membrane was immersed in PX for 24 h to ensure that the porous film of hollow fibers was fully saturated by PX. The aqueous solution was pumped through the lumen side by using a digital single-piston solvent pump (Lab-Alliance Series I, USA), while the extractant flowed countercurrently through the shell side. The flow rates were calibrated by measuring the outlet flow volumes over a certain time interval with an overall

uncertainty of $\pm 1\%$. A slight over pressure (about 5 kPa) between the lumen and shell sides at any axial position was maintained by adjusting the value on the lumen outlet pipeline. The temperature was controlled by immersing the membrane module in a water bath at the assigned temperature.

Table 1 Specifications of the hollow fiber and membrane module

Parameter	Value
Effective hollow fiber length, L (m)	0.8
Fiber inner radius, r_1 (μm)	195 ± 10
Fiber outer radius, r_2 (μm)	245 ± 10
Maximum diameter of pores, d_p (nm)	200
Membrane porosity, ε	0.45
Membrane tortuosity, τ	2.2
Membrane-water contact angle, θ_c ($^\circ$)	120
Membrane-water interfacial tension, γ (N/m)	0.05
Module inner radius, r_m (mm)	3.0
Number of fiber in the module, n	59
Packing density*, ϕ	0.39

* Ratio of the volume of the hollow fibers in the module to the volume of the membrane module

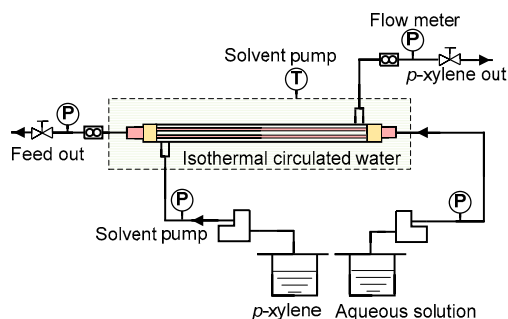


Fig. 1 Schematic diagram of the NDSE experimental setup

The following operating parameters were investigated: extraction time t_e (or contact time, represented by the aqueous residence time in the lumen side for a single pass), aqueous/organic volumetric flow ratio (a/o), initial PT acid concentration (C_f), and temperature (T). The extraction time in experiments ranged from 20 to 70 s, the a/o from 3.0 to 9.0, the initial PT acid concentration from 300 to 900 g/m^3 , and the temperature from 308.2 to 328.2 K. Pre-experiments indicated that an extraction time of 70 s was sufficient to reduce the PT acid concentration to the re-use standard. The above ranges cover available conditions of the existing PTA process while

taking into account the appropriate NDSE operating conditions to realize the re-use of water raffinate.

The lumen and shell side outlet streams were sampled after the NDSE experiments reached a steady state (after running for about 20 min), and the PT acid concentration of the solutions was analyzed by means of a high performance liquid chromatography (HPLC). Details of the analytical method can be found in Kong *et al.* (2013). Three parallel samples were prepared and analyzed for each experimental run to evaluate the relative deviation, which was shown to be less than 1%. The data presented in Section 4.1 are the mean values obtained in the duplicate experiments. The mass conservation of PT acid between the outlet streams and the aqueous inlet stream was also measured and was found to have a relative deviation of less than 1%.

3 Theory

3.1 Model formulation

A membrane module usually contains a huge number of hollow fibers (about 10000 to 70000). However, the modeling of the membrane module can be equivalently transformed into the case of a single fiber surrounded by a concentric cylinder solvent flow layer (Fig. 2, see ‘‘Happel’s free surface model’’ below). The aqueous phase flows in the lumen side and the organic phase in the shell side. Both are assumed to be fully developed countercurrent laminar flows. The aqueous phase enters at $z=0$. The hydrophobic membrane is considered non-wetted with aqueous solution but filled with PX in the micropores. An aqueous/organic interface therefore forms at the mouth of membrane pores adjacent to the lumen side. PT acid in the lumen aqueous phase diffuses firstly to the interface, where it is extracted by the organic phase, then permeates through the membrane, spreads to the shell side, and finally is brought out by the organic phase.

The model developed to simulate the mass transport in NDSE contains solutions of the continuity equations in all the sub-regions, i.e., the lumen side, the membrane, and the shell side, with appropriate velocity distributions. The differential form of mass balance (also called the convection and diffusion equation) can be written as (Bringas *et al.*, 2009)

$$V_i \frac{\partial C_i}{\partial z} = D_i \frac{1}{r} \frac{\partial}{\partial r} \left(r \frac{\partial C_i}{\partial r} \right), \quad (1)$$

where V , C , and D with subscript i refer to the velocity distribution, the concentration of PT acid, and the diffusivity and physical property in the i th sub-region, respectively; z and r are the axes of cylindrical coordinates. The term on the left-hand side illustrates the axial convective transport mass flux of PT acid, while that on the right-hand side represents the radial diffusive transport mass flux. Note that the axial diffusion is supposed to be negligible.

The velocity distribution in the lumen side follows Newtonian laminar flow (Eq. (3) in Table 2). In the porous membrane, where the velocity is zero, the mass transport is by diffusion only. Hence, the concentration profile can be expressed analytically by

$$C_m = \left(C_m|_{r=r_2} - C_m|_{r=r_1} \right) \ln(r/r_1) / \ln(r_2/r_1) + C_m|_{r=r_1}, \quad (2)$$

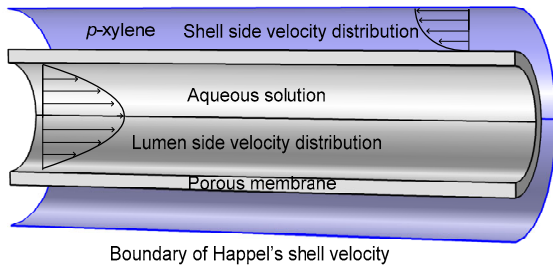


Fig. 2 Transport scheme of PT acid in a countercurrent flow pattern with Happel's free surface model

where r_1 and r_2 are the fiber inner and outer radii, and the subscript m denotes the quantity in the membrane. In the shell side, Happel's free surface model (Happel, 1959) is adopted to describe the shell side velocity V_o (Eqs. (4a) and (4b) in Table 2). This model simplifies the shell side into a concentric cylinder flow layer surrounding the fiber core. The volumetric rate of the shell side is assumed to be evenly distributed around each fiber with a slip condition at the outer interface of the shell side.

The boundary conditions of the lumen and shell sides are expressed by Eqs. (5a)–(6c) in Table 2. Note that the concentrations on both sides at the interface $r=r_1$ satisfy the phase equilibrium relationship $C_m=f(C_a)$, which will be discussed in Section 3.2.1.

3.2 Model parameters

3.2.1 Estimation of phase equilibrium parameters and diffusivities

The phase equilibrium relationship of PT acid in PX and water phases has been described by the non-random two liquid (NRTL) activity coefficient model (Kong et al., 2013). The model, however, has a complicated expression. For simplicity in calculation, a quadratic form of the phase equilibrium relationship has been re-correlated, which also shows high fitting precision ($R^2>0.997$, Fig. 3).

$$[C_o] = a[C_a] + b[C_a]^2, \quad (7)$$

Table 2 Mathematical expressions in relation to Eq. (1)

Mathematical term	Mathematical expression	
	Lumen side	Shell side
Velocity distribution	$V_a = 2\bar{V}_a \left(1 - (r/r_1)^2 \right)$ (3)	$V_o = \frac{2\bar{V}_o (r_3^2 - r_2^2) (r_2^2 - r^2 + 2r_3^2 \ln(r/r_2))}{4r_2^2 r_3^2 - r_2^4 - 3r_3^4 + 4r_3^4 \ln(r_3/r_2)}$, (4a) $r_3 = \phi^{-0.5} r_2$ (4b)
Boundary condition	$r = 0: \partial C_a / \partial r = 0,$ (5a)	$r = r_3: \partial C_o / \partial r = 0,$ (6a)
	$r = r_1: D_a \frac{\partial C_a}{\partial r} = D_m \frac{\partial C_m}{\partial r}$ $= D_m (C_m _{r=r_2} - C_m) / (r_1 \ln(r_2/r_1)),$ (5b)	$r = r_2: D_o \frac{\partial C_o}{\partial r} = D_m \frac{\partial C_m}{\partial r}$ $= D_m (C_m - C_m _{r=r_1}) / (r_2 \ln(r_2/r_1)),$ (6b)
	$C_m = f(C_a),$	$C_o = C_m,$
	$z = 0: C_a = C_f$ (5c)	$z = L: C_o = 0$ (6c)

Note: r_3 , ϕ , and \bar{V} stand for the free surface radius, the packing density of a membrane module, and the mean velocity, respectively; subscripts a and o refer to physical property in lumen and shell side sub-regions, respectively

where $[C_a]$ and $[C_o]$ represent equilibrium concentrations of PT acid in water and PX, respectively. Values of a and b are listed in Table 3. A comparison between experimental and calculated results is shown in Fig. 3.

Table 3 Equilibrium parameters in Eq. (7) and diffusivities of PT acid in water and PX phases

Temperature (K)	a	b (m^3/mol)	D_a ($\times 10^{-9} \text{m}^2/\text{s}$)	D_o ($\times 10^{-9} \text{m}^2/\text{s}$)
303.15	-0.2888	8.460	0.8708	2.047
313.15	0.3515	6.234	1.156	2.415
323.15	0.6997	4.581	1.441	2.783
333.15	1.186	3.243	1.726	3.152
343.15	1.486	2.337	2.011	3.519
353.15	1.762	1.525	2.296	3.888

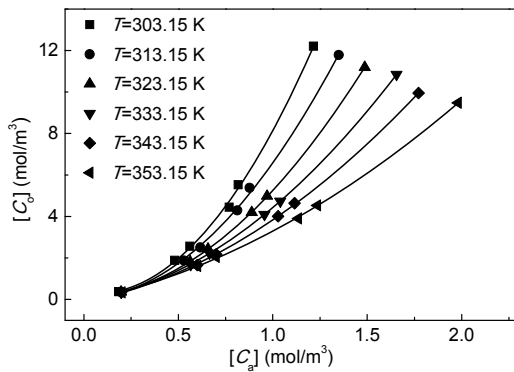


Fig. 3 Quadratic form of phase equilibrium relationship between water and PX for PT acid. Points are experimental data from Kong *et al.* (2013), and lines are calculation results from Eq. (7)

For convenience, in the following computation on temperature dependence, the values of a and b can be further correlated with temperature ($R^2 > 0.995$) by

$$a = -51.05 + 0.2767T - 3.601 \times 10^{-4} T^2, \quad (8a)$$

$$b = 177.6 - 0.7254T + 1.820 \times 10^{-6} T^3, \quad (8b)$$

where T is the value of thermodynamic temperature.

Diffusivities of PT acid in water (D_a) and PX (D_o) are calculated using the Wilke-Chang equation (Wilke and Chang, 1955). The results are listed in Table 3. The diffusivity of PT acid in membrane pores is calculated by multiplying D_o by the membrane porosity (ϵ) and dividing by membrane tortu-

osity (τ). Moreover, the temperature dependence of diffusivities can be correlated ($R^2 > 0.999$) by

$$D_a = -7.769 \times 10^{-9} + 2.850 \times 10^{-11} T, \quad (9a)$$

$$D_o = -9.115 \times 10^{-9} + 3.862 \times 10^{-11} T. \quad (9b)$$

3.2.2 Estimation of pressure drops and breakthrough pressure

To avoid penetration of PX through the membrane layer into the lumen side, the aqueous solution needs to maintain a higher pressure than the shell side at any axial position. The pressure profiles along the lumen and shell sides should therefore be calculated to estimate the maximum pressure difference. Following Bieluszka *et al.* (2014), the pressure drops in the lumen side Δp_a and the shell side Δp_o can be calculated by

$$\Delta p_a = -\frac{8\bar{V}_a \mu_a z}{r_1^2}, \quad (10a)$$

$$\Delta p_o = -\frac{8(r_3^2 - r_2^2)\bar{V}_o \mu_o z}{4r_2^2 r_3^2 - r_2^4 - 3r_3^4 + 4r_3^4 \ln(r_3/r_2)}, \quad (10b)$$

where μ is the viscosity of the liquid.

The pressure difference between the water and PX phases, however, must be larger than zero but smaller than the breakthrough pressure P_{cr} . For the countercurrent flow of aqueous and organic phases, the sum of the pressure differences should satisfy the following restriction:

$$\Delta p_a + \Delta p_o < P_{cr}. \quad (11)$$

Overpressure will lead to the aqueous phase leaking through the membrane into the shell side. P_{cr} can be estimated using the Young-Laplace equation (Drioli and Giorno, 2010):

$$P_{cr} = -\frac{4\Theta\gamma \cos \theta_c}{d_p}, \quad (12)$$

where Θ , γ , θ_c , and d_p are the geometric factor (equal to 1 for cylindrical pores), the interfacial tension, the liquid-solid contact angle, and the maximum diameter of pores, respectively.

3.3 Numerical solution of model equations

The model equations are hard to solve analytically due to the non-linear equilibrium relationship on the boundary conditions Eq. (7). So the models in the lumen and shell sub-regions were solved numerically using COMSOL software (version 4.3a) in a 2D axi-symmetric coordinate system. The sub-regions should be scaled up due to the large difference between the r - and z -directions. The lumen and shell sub-regions were meshed automatically with mesh generated by COMSOL, having quite a fine mesh near all the boundaries/interfaces by adopting the boundary distribution. Note that the membrane sub-region was not meshed. The concentration profile of the membrane was calculated from Eq. (2) after the computation of the other two sub-regions. Finite element analysis is combined with error control using the numerical solver of SPOOLES with a computational time of about 20 min and a relative tolerance of less than 10^{-6} .

To demonstrate the accuracy of numerical programming, a case of the classical Graetz problem was solved and compared with the analytical solution. For the lumen side with wall concentration equal to zero, the analytical solution takes the form of a Fourier series (Graetz, 1885):

$$C(r, z) = \sum_{n=1}^{\infty} A_n Y_n(r) \exp(-\lambda_n^2 z), \quad (13)$$

where A_n , Y_n , and λ_n are the associated constant, the eigenfunction, and the eigenvalue, respectively. Fig. 4 shows the numerical and analytical solutions of dimensionless concentration profiles ($C_f=1$). The relative errors between the two solutions are less than 1×10^{-4} , which means that the numerical algorithm is sufficiently accurate.

A grid independence test was conducted to check the mass conservation of PT acid in the sub-regions. The number of cells was varied from 80000 to 120000. After 100000 cells, a further increase in cell number led to a less than 0.1% change in the mass conservation. Considering both computational time and accuracy, all the computations were conducted with 100000 cells.

To evaluate NDSE performance, three indexes were defined as follows, and used as measures of the

aqueous outlet PT acid concentration (C_{out}), efficiency of the membrane module (E_m), and efficiency of the solvent (E_s):

$$C_{out} = \frac{\int_0^{r_1} r V_a C_a|_{z=1} dr}{\int_0^{r_1} r V_a dr}, \quad (14a)$$

$$E_m = (C_f - C_{out}) u_a / V_m, \quad (14b)$$

$$E_s = C_{out,o} / C^* = (a/o)(C_f - C_{out}) / (aC_f + bC_f^2), \quad (14c)$$

where u_a is the overall volumetric flow rate of the aqueous solution in a module, V_m is the volume of the module, and C_f , $C_{out,o}$, and C^* are the initial feed PT acid concentration, the organic outlet PT acid concentration, and equilibrium concentration, respectively. C_{out} measures the degree of wastewater purification, which should be lower than 100 g/m^3 for re-use in the PTA process. E_m denotes the capacity of the module. A higher value of E_m means the membrane module runs more efficiently. E_s represents the efficiency of solvent usage. A higher value of E_s means less solvent is needed in extraction. The maximum of 1.0 denotes the limit of the extraction at aqueous/organic equilibrium.

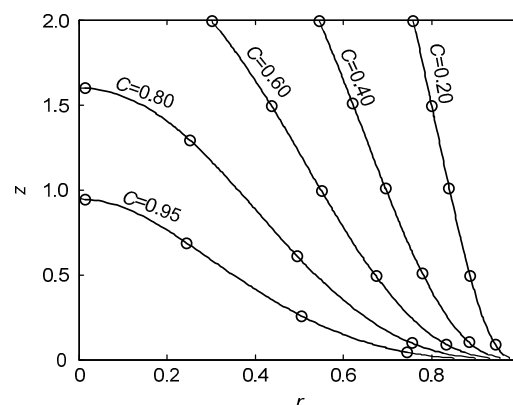


Fig. 4 Comparison of numerical and analytical solutions for the Graetz problem. Points are from the analytical solution, and lines are numerical results

4 Results and discussion

4.1 Experimental results

Figs. 5–7 show the experimental results for the aqueous outlet PT acid concentration (C_{out}) with

various operating parameters. Fig. 5 illustrates the effects of the extraction time (t_e) and initial PT acid concentration (C_f). C_{out} decreases dramatically from 1.30 to 0.585 mol/m³ as t_e increases from 20 to 70 s ($C_f=3.67$ mol/m³), indicating that t_e is a very sensitive parameter. This is expected for a hydrophobic membrane wetted by an extractant with a large partition coefficient (Shen *et al.*, 2009). A longer extraction time indicates a longer axial conventional time compared with the radial diffusion time, so a higher proportion of PT acid will diffuse to the organic phase leading to better extraction performance. When t_e is longer than 60 s, C_{out} can be reduced to lower than 0.734 mol/m³ (100 g/m³) for water re-use in all cases. Thus, 20–70 s is a suitable range for t_e from a practical point of view. A remarkable rise in the feed concentration C_f (300–900 g/m³) slightly increases the outlet concentration C_{out} (72.3–89.2 g/m³, $t_e=70$ s), which means that the higher is the impurity concentration in the wastewater, the more effective is the NDSE method. Younas *et al.* (2008) suggested that the higher extraction rate caused by a higher initial concentration is more obvious with a short extraction time, and after a sufficiently long time the influence of the initial concentration on the aqueous outlet concentration can be negligible. This can be further explained by Fig. 3 which shows that a higher C_f will lead to a higher partition coefficient ($m=[C_o]/[C_a]$) and overall mass transport coefficient (Section 4.2), and so will facilitate the mass transport, but will tend to be unremarkable in terms of the decrease in the aqueous PT acid concentration.

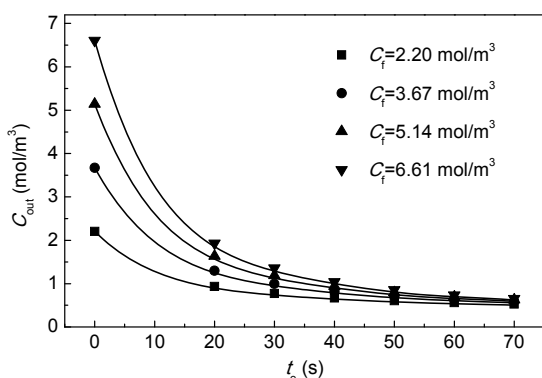


Fig. 5 Effects of extraction time (t_e) and initial PT acid concentration (C_f) on the aqueous outlet PT acid concentration (C_{out}) with $a/o=9.0$ and $T=318$ K (lines are simulation results)

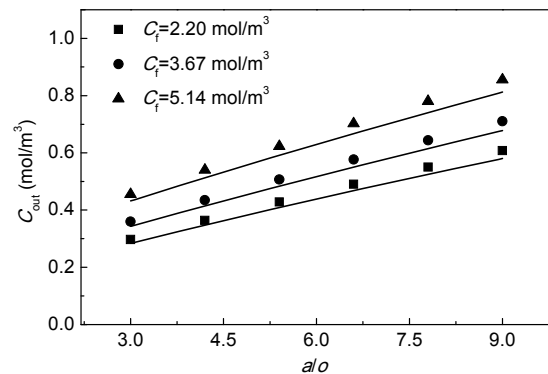


Fig. 6 Effects of volumetric ratio (a/o) and initial PT acid concentration (C_f) on the aqueous outlet PT acid concentration (C_{out}) with $t_e=50$ s and $T=318$ K (lines are simulation results)

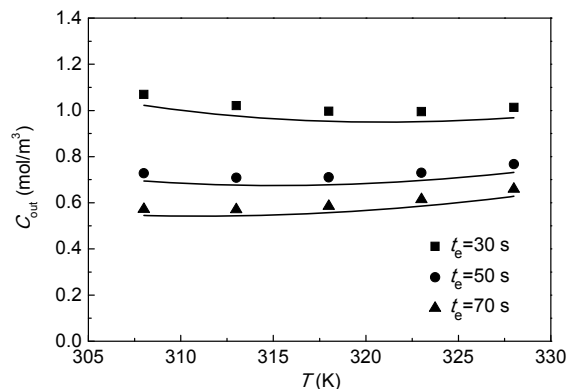


Fig. 7 Effects of temperature (T) and extraction time (t_e) on the aqueous outlet PT acid concentration (C_{out}) with $a/o=9.0$ and $C_f=3.67$ mol/m³ (500 g/m³) (lines are simulation results)

Fig. 6 shows the variation in C_{out} with various aqueous/organic volumetric flow ratios (a/o) and C_f values. C_{out} exhibits a notably near-linear increase from 49.0 to 96.7 g/m³ ($C_f=3.67$ mol/m³) with a/o in all the experiments. The influence of a/o is because of the less extractant being available for a higher ratio of feed to PX, as already noted in previous studies (Agarwal *et al.*, 2013; 2014). A smaller a/o will therefore improve the performance of NDSE but increase the cost of solvent use. In addition, C_{out} is not as sensitive to a/o as it is to the extraction time.

Fig. 7 indicates the effects of temperature on C_{out} with different extraction time. For a certain t_e , C_{out} seems to have a minimum value in the temperature range investigated. C_{out} changes from 99.0 to 96.5 g/m³ then to 104 g/m³ with T varying from 308

to 313 K then to 328 K, respectively ($t_e=50$ s). Temperature rise has two opposing effects on the extraction: accelerating the diffusion of PT acid or the rate of extraction, and decreasing the equilibrium partition coefficient m or extraction capacity of the PX phase. Therefore, there should be an optimal temperature for a certain t_e . This phenomenon is further investigated over a wider range by computational simulation in Section 4.4.

The extraction process under experimental conditions was simulated by Eqs. (1)–(9) to validate the model and parameters. A comparison between computed and experimental results is shown in Figs. 5–7. The relative errors between them are less than 6%, which demonstrates that the model parameters were all properly estimated. The positive deviation between the experimental and computational C_{out} may come from the non-ideality of velocity distributions in the entrance of the hollow fiber. In the following sections, the simulation results are used to investigate further the impacts of a wide range of operating conditions, so as to select proper extracting conditions.

4.2 Concentration profiles in all sub-regions

The concentration profiles were calculated under typical industrial operating conditions: $u_a=0.204$ m³/h, $t_e=50$ s, $C_f=6.61$ mol/m³ (900 g/m³), $a/o=9.0$, $T=318$ K, $r_1=200$ μ m, $r_2=250$ μ m, $r_3=400$ μ m, $r_m=60$ mm (module inner radius), $n=22\,522$, $L=1.0$ m, $\phi=0.391$, $\varepsilon=0.45$, and $\tau=2.2$. The aqueous outlet concentration of PT acid in this case is 0.704 mol/m³ (95.9 g/m³). Fig. 8 depicts the PT acid concentration profiles in three parts representing, from left to right, the lumen side, the membrane, and the shell side, respectively. The PT acid concentration in aqueous solution notably decreases along the radial direction from the center to the membrane wall of the hollow fiber. At the aqueous-membrane interface the concentration shows an abrupt jump from the aqueous phase to the PX phase, as a result of a much higher partition ratio ($m \gg 1$) of PT acid in the PX phase than that in the aqueous phase. The PT acid concentration in the PX phase, C_o , maintains a high platform on the membrane and shell side, but decreases slightly along the radial direction on the shell side. In the axial direction, the concentrations of C_a and C_o decrease dramatically as a result of countercurrent

contact of aqueous and organic phases. The impurity PT acid transfers from the lumen aqueous phase to the membrane organic phase, then penetrates the membrane, and is swept out from the module by PX.

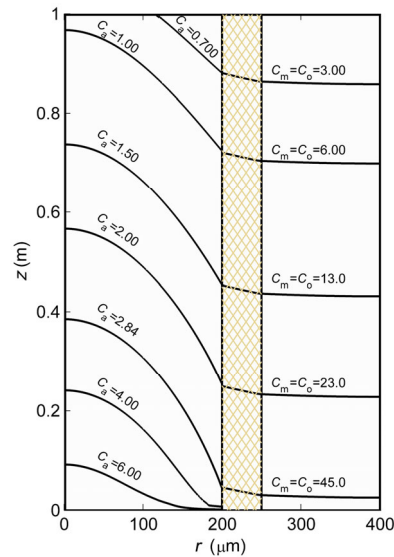


Fig. 8 PT acid concentration profiles (mol/m³) in all the sub-regions under typical industrial operating conditions. The three parts, from left to right, represent the lumen side, the membrane, and the shell side, respectively. At the aqueous inlet boundary $z=0$ m, while at the organic inlet boundary $z=1$ m

To quantitatively evaluate the resistances in the sub-regions, the individual mass transfer coefficients (k_i) in all the sub-regions are introduced as follows (McCabe *et al.*, 1993):

$$\begin{cases} k_a \approx D_a / r_1, \\ k_m \approx D_m / (r_2 - r_1), \\ k_o \approx D_o / (r_3 - r_2). \end{cases} \quad (15)$$

The contributions of k_i to the aqueous solution based on the overall mass transfer coefficient (K_a) can be calculated by the well-known resistance-in-series model (Gameiro *et al.*, 2008):

$$\frac{1}{K_a} = \frac{1}{k_a} + \frac{r_1}{k_m m r_{lm}} + \frac{r_1}{k_o m r_2}, \quad (16)$$

where r_{lm} is the logarithmic mean radius of membrane. m represents the slope of a linear-relationship

partition coefficient equation as

$$m = \left. \frac{dC_m}{dC_a} \right|_{r=r_1} = a + 2bC_a \Big|_{r=r_1}. \quad (17)$$

In the case shown in Fig. 8, the values of $1/k_a$, $r_1/(k_m m r_{1m})$, and $r_1/(k_o m r_2)$ on the right hand side of Eq.(16) at $z=0.5$ m are 1.55×10^5 , 5.37×10^3 , and 2.97×10^3 , respectively. The order of magnitude indicates that the aqueous mass transfer resistance predominates, i.e., $K_a \approx k_a$, which means the rate determining step of the overall mass transfer process is in the lumen side. This situation is similar to that described by Kiani *et al.*(1984) as a “high value of m ”. Fig. 3 shows that m is in the range of 4–12 which means most PT acid initially in the aqueous phase tends to concentrate in the organic phase when contacting PX. As a result, at the contacting surface of the boundary between the lumen side and membrane, PT acid in the aqueous phase will decrease dramatically while the concentration gradient will become steep. In the lumen side, there is purely axial laminar flow without any radial or tangential velocity. The only radial mass transfer mechanism is molecular diffusion. Table 3 shows that the PT acid diffusivity D_a is of the order of 10^{-9} m²/s, so low diffusivity restricts radial mass transfer in the lumen side, which thereby becomes the rate determining step of the overall mass transfer process. Note that in Fig. 6, a/o still shows a relatively notable effect on C_{out} with constant t_e , which means that flow in the shell side is also important in affecting the aqueous/solvent ratio.

4.3 Influence of membrane parameters

The effects of the fiber inner radius and porosity-to-tortuosity ratio (ε/τ) on NDSE performance need to be investigated for selection of membrane modules. Enlarging r_1 will decrease the pressure drop in the lumen side and hence the pumping costs (Wickramasinghe *et al.*, 1991), as well as enhance the strength of the fiber, while ε/τ varies among different commercial membrane products. Usually, when designing a membrane module, the packing density of hollow fibers (defined as the volume fraction of hollow fibers occupied in a module) is a constant value as high as possible (about 0.40 for a module with high flow rate, provided by the mem-

brane supplier), and the wastewater treatment load of a module should be set unchanged. Keeping packing density and load constant, increasing r_1 means prolonging the extraction time, reducing the number of hollow fibers and the aqueous-organic contact area. Simulations were run under the typical conditions $u_a=0.204$ m³/h, $a/o=9.0$, $C_f=6.61$ mol/m³ (900 g/m³), $T=318$ K, $\Delta r_2=r_2-r_1=50$ μ m, $r_m=60$ mm, $L=1.0$ m, and $\phi=0.391$. Note that usually the length of fiber for commercial products is 1.0 m, so L was set as 1.0 m in all simulations. To maintain a constant membrane thickness (50 μ m), the free surface radii r_3 and r_1 were varied simultaneously. The ε/τ ranged from 0.067 to 0.45, corresponding to the typical values reported by Gabelman and Hwang (1999).

Simulation results (Fig. 9) show the variation in C_{out} with various values of r_1 and ε/τ . A smaller r_1 results in a lower C_{out} , and higher efficiencies of E_m and E_s calculated from Eqs. (14b) and (14c). A decrease in r_1 leads to two opposite effects: a shorter radial distance and larger contact area for PT acid diffusion, and a shorter extraction time when keeping packing density and flow rate unchanged (e.g., $r_1=150$ μ m, $t_e=43.9$ s; $r_1=300$ μ m, $t_e=57.3$ s). The former becomes predominant (Fig. 9). This result seems to contradict the findings of Younas *et al.* (2008), who observed the opposite effect of r_1 for NDSE of aroma compounds, i.e., a larger inner radius increased the mass transfer rate. The discrepancy originates from differences in the conditions in the two studies. In the study of Younas *et al.* (2008) the number of fibers was kept constant while the packing density was allowed to vary, but in this study, the fiber packing density was kept constant while the number of fibers varied. At a fixed overall flow rate and fiber number, an increase in fiber radius increases extraction time and packing density, both of which undoubtedly promote mass transfer in extraction, as in the case of Younas *et al.* (2008).

Fig. 9 also shows that C_{out} decreases with a rise in ε/τ . For a large ε/τ of 0.20–0.45, the influence becomes unremarkable. A similar trend is found for E_m and E_s . A large ε/τ leads to high diffusivity in the membrane. However, the membrane resistance is not a dominant factor for mass transfer, so the effect is limited. Considering the balance between NDSE performance and fiber lifetime, an r_1 of 200–250 μ m is suggested, while ε/τ should be larger than 0.20.

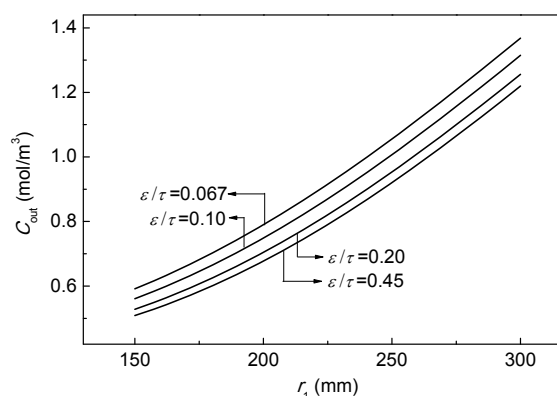


Fig. 9 Effects of the fiber inner radius (r_1) and porosity-to-tortuosity ratio (ϵ/τ) on the aqueous outlet PT acid concentration (C_{out}), keeping the fiber packing density, membrane thickness, and overall volumetric flow rate unchanged

4.4 Influence of operating parameters

The ratio of aqueous and organic phase volumetric flow rates a/o and temperature are the most important operating parameters, in addition to extraction time, which should be carefully designed in view of the required effluent PT acid content, industrial restrictions, and the cost of NDSE. The maximum PX amount available in a conventional PTA plant is 1/3 of the wastewater, which means a/o should be larger than 3. The temperature of wastewater in practice is in the range of 30–80 °C. A lower temperature extends the lifetime of the hollow fiber, but increases cooling costs.

Fig. 10 illustrates the effects of the t_e and a/o on the aqueous outlet concentration. All parameters except t_e , u_a , and a/o were fixed at the typical values used in Section 4.2. As expected, C_{out} decreases with t_e and increases with a/o . Prolonging t_e will facilitate the radial transport of PT acid from aqueous solution to the membrane, while decreasing a/o would enhance the axial convection in the shell side, both of which reduce C_{out} . t_e is more sensitive over short (20–60 s) than over long periods. In view of the C_{out} requirement, treating efficiency and cost, t_e should be set around 60 s in the design and an a/o should be selected that is as large as possible near the contour of C_{out} 0.734 mol/m³ (100 g/m³).

Fig. 11 shows the variation in the module efficiency E_m with t_e and a/o . E_m dramatically decreases with t_e and slightly declines with a/o , which is easy

to understand from Eq. (14b) as E_m is directly proportional to $(C_f - C_{out})$ and inversely proportional to the aqueous residence time (extraction time t_e). Changes in t_e and a/o in the range only slightly alter the concentration difference ($C_f - C_{out}$) which cannot catch up with $1/t_e$. A short time means high efficiency and outlet PT acid content. So there are contradictory requirements between water cleanness and treatment efficiency that require a compromise in the design of NDSE.

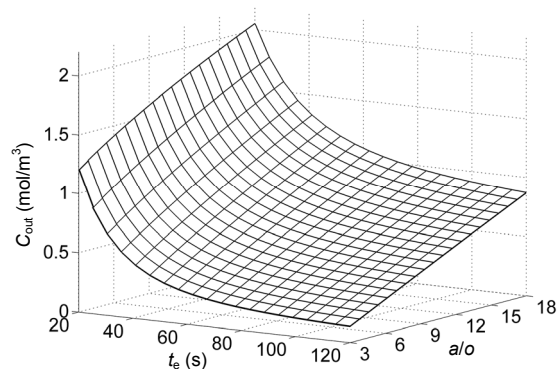


Fig. 10 Effects of the extraction time (t_e) in the lumen side and volumetric ratio (a/o) on the aqueous outlet PT acid concentration (C_{out})

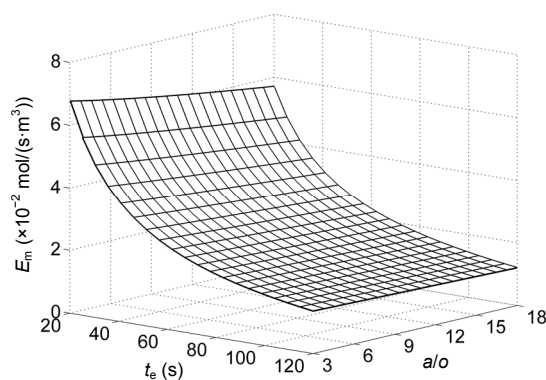


Fig. 11 Effects of the extraction time (t_e) in the lumen side and volumetric ratio (a/o) on the efficiency of the membrane module (E_m)

Fig. 12 depicts the variation in solvent efficiency E_s with t_e and a/o . E_s is between 0.07 and 0.44 in the considered range, far smaller than 1.0, which means the extractant PX was in the unsaturated state in the purification of the wastewater. a/o shows a remarkable effect on E_s while t_e seems to have less effect, which is clear from Eq. (14c). Less solvent

usage means a lower cost and a higher impurity content. A compromise choice for the water/solvent ratio seems appropriate at an a/o of about 9.0.

The pressure difference between the lumen and shell sides and the breakthrough pressure were calculated to prevent breakthrough of both PX and aqueous phases in the t_e ranges of interest. The results show the maximum pressure difference is 6.62 kPa while $t_e=20$ s and $a/o=3.0$, which is far beyond the breakthrough pressure of 500 kPa. Moreover, the pressure drop along the membrane module is not appreciable, which can reduce the operating costs of the process (Fadaei *et al.*, 2011).

The effect of temperature on C_{out} is shown in Fig. 13. In the simulation, other parameters used were the typical values described in Section 4.2. According to Eqs. (14b) and (14c), E_m and E_s will simultaneously reach maximum values when C_{out} is at the minimum point for a certain t_e . A close inspection

of Fig. 13 shows that the optimal temperature moves towards a higher value as t_e decreases (from 306 to 328 K with t_e reducing from 110 to 20 s). Compared with Fig. 7, the existence of the C_{out} minimum and shift tendency is shown more clearly in Fig. 13, especially for the case of a short extraction time. As pointed out in Section 4.1, a temperature rise will accelerate PT acid diffusion but decrease the solvent extraction capacity. The C_{out} minimum is a balance between these two opposing effects. This phenomenon become more evident in the situation of a short extraction time where mass transfer proceeds faster, and the kinetic and thermodynamic factors dominate at low and high temperature intervals, respectively. For the t_e and a/o suggested above, an appropriate T was chosen as 318 K.

5 Conclusions

NDSE with PX as extractant to recover both PT acid and water from PTA wastewater was shown to be feasible and effective by means of experiment and model simulation. The effects of membrane and operating parameters t_e , a/o , T , C_f , r_1 , and ε/τ on the PT acid content in the raffinate C_{out} and the membrane, and on solvent efficiencies E_m and E_s , were experimentally and numerically investigated. The rate determining step of mass transport was found to be within the aqueous solution. The extraction time t_e and fiber radius r_1 are, therefore, the two parameters to which C_{out} is most sensitive. Shrinkage of the radius r_1 can remarkably accelerate PT acid transport, decrease C_{out} , and enhance the extraction efficiency E_m at the cost of increasing the pressure drop and shortening the membrane lifetime. Prolonging t_e will reduce PT acid content in raffinate at the cost of reducing membrane efficiency. A larger a/o ratio results in less extractant usage but increasing PT acid content, and a/o shows near-linear influences on C_{out} and solvent efficiency E_s , but has little effect on E_m . Temperature has opposing effects on mass transport: a higher T increases PT acid diffusivities, but reduces the partition coefficient in the organic phase. Therefore, there exists an optimal T value for NDSE performance. The optimal temperature moves towards a higher value as t_e decreases. A higher feed PT acid concentration C_f will enhance the extraction efficiency and slightly increase C_{out} . In view of the availability in industrial PTA processes and the

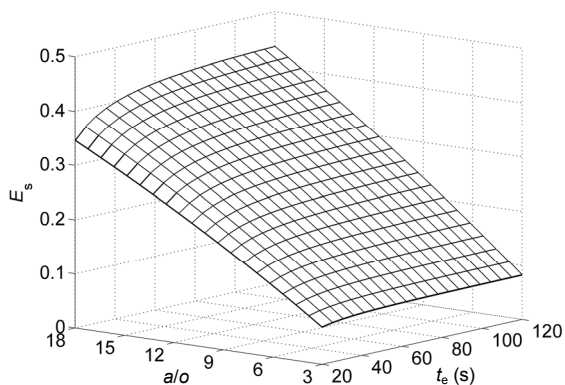


Fig. 12 Effects of the extraction time (t_e) in the lumen side and volumetric ratio (a/o) on solvent efficiency (E_s)

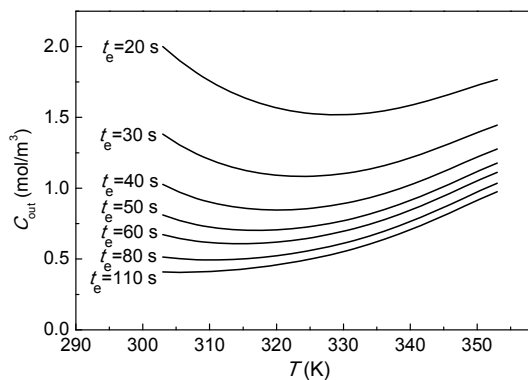


Fig. 13 Effects of the operating temperature (T) and the extraction time (t_e) on the aqueous outlet PT acid concentration (C_{out})

necessary compromise between water cleanness and extraction cost, the membrane and operating parameters appropriate for industrial design are suggested as follows: $t_e=50-60$ s, $a/o=9.0$, $T=318$ K, $r_1=200-250$ μm , and $\varepsilon/\tau=0.20-0.45$. Under these conditions, PTA wastewater can be purified and re-used, together with PT acid recovery, with acceptable efficiencies of the membrane module and solvent.

References

- Agarwal, S., Reis, M.T.A., Ismael, M.R.C., et al., 2013. Application of pseudo-emulsion based hollow fibre strip dispersion (PEHFSD) for the recovery of copper from sulphate solutions. *Separation and Purification Technology*, **102**:103-110.
<http://dx.doi.org/10.1016/j.seppur.2012.09.026>
- Agarwal, S., Reis, M.T.A., Ismael, M.R.C., et al., 2014. Zinc extraction with ionquest 801 using pseudo-emulsion based hollow fibre strip dispersion technique. *Separation and Purification Technology*, **127**:149-156.
<http://dx.doi.org/10.1016/j.seppur.2014.02.039>
- Barati, F., Ghadiri, M., Ghasemi, R., et al., 2014. CFD simulation and modeling of membrane-assisted separation of organic compounds from wastewater. *Chemical Engineering & Technology*, **37**(1):81-86.
<http://dx.doi.org/10.1002/ceat.201300278>
- Bieluszka, P., Zakrzewska, G., Chajduk, E., et al., 2014. Liquid-liquid extraction of uranium (VI) in the system with a membrane contactor. *Journal of Radioanalytical and Nuclear Chemistry*, **299**(1):611-619.
<http://dx.doi.org/10.1007/s10967-013-2796-0>
- Bringas, E., San Román, M.F., Irabien, J.A., et al., 2009. An overview of the mathematical modelling of liquid membrane separation processes in hollow fibre contactors. *Journal of Chemical Technology and Biotechnology*, **84**(11):1583-1614.
<http://dx.doi.org/10.1002/jctb.2231>
- Daramola, M.O., Aransiola, E.F., Adeogun, A.G., 2011. Comparative study of thermophilic and mesophilic anaerobic treatment of purified terephthalic acid (PTA) wastewater. *Natural Science*, **3**(5):371-378.
<http://dx.doi.org/10.4236/ns.2011.35050>
- Dixit, S., Chinchale, R., Govalkar, S., et al., 2013. A mathematical model for size and number scale up of hollow fiber modules for the recovery of uranium from acidic nuclear waste using the DLM technique. *Separation Science and Technology*, **48**(16):2444-2453.
<http://dx.doi.org/10.1080/01496395.2013.807825>
- Đorđević, J.S., Vladisavljević, G.T., Trtić-Petrović, T.M., 2014. Removal of the selected pesticides from a water solution by applying hollow fiber liquid-liquid membrane extraction. *Industrial & Engineering Chemistry Research*, **53**(12):4861-4870.
<http://dx.doi.org/10.1021/ie404210k>
- Drioli, E., Giorno, L., 2010. *Comprehensive Membrane Science and Engineering*. Elsevier, UK.
- Fadaei, F., Shirazian, S., Ashrafizadeh, S.N., 2011. Mass transfer simulation of solvent extraction in hollow-fiber membrane contactors. *Desalination*, **275**(1-3):126-132.
<http://dx.doi.org/10.1016/j.desal.2011.02.039>
- Gabelman, A., Hwang, S.T., 1999. Hollow fiber membrane contactors. *Journal of Membrane Science*, **159**(1-2):61-106.
[http://dx.doi.org/10.1016/S0376-7388\(99\)00040-X](http://dx.doi.org/10.1016/S0376-7388(99)00040-X)
- Gameiro, M.L.F., Ismael, M.R.C., Reis, M.T.A., et al., 2008. Recovery of copper from ammoniacal medium using liquid membranes with LIX 54. *Separation and Purification Technology*, **63**(2):287-296.
<http://dx.doi.org/10.1016/j.seppur.2008.05.009>
- Graetz, L., 1885. Ueber die wärmeleitungsfähigkeit von flüssigkeiten. *Annalen der Physik*, **261**(7):337-357 (in German).
<http://dx.doi.org/10.1002/andp.18852610702>
- Gupta, S., Chakraborty, M., Murthy, Z., 2014. Performance study of hollow fiber supported liquid membrane system for the separation of bisphenol A from aqueous solutions. *Journal of Industrial and Engineering Chemistry*, **20**(4): 2138-2145.
<http://dx.doi.org/10.1016/j.jiec.2013.09.043>
- Hao, Z., Vilt, M.E., Wang, Z., et al., 2014. Supported liquid membranes with feed dispersion for recovery of cephalixin. *Journal of Membrane Science*, **468**:423-431.
<http://dx.doi.org/10.1016/j.memsci.2014.06.009>
- Happel, J., 1959. Viscous flow relative to arrays of cylinders. *AIChE Journal*, **5**(2):174-177.
<http://dx.doi.org/10.1002/aic.690050211>
- Kiani, A., Bhave, R.R., Sirkar, K.K., 1984. Solvent extraction with immobilized interfaces in a microporous hydrophobic membrane. *Journal of Membrane Science*, **20**(2): 125-145.
[http://dx.doi.org/10.1016/S0376-7388\(00\)81328-9](http://dx.doi.org/10.1016/S0376-7388(00)81328-9)
- Kleerebezem, R., Beckers, J., Hulshoff Pol, L.W., et al., 2005. High rate treatment of terephthalic acid production wastewater in a two-stage anaerobic bioreactor. *Biotechnology and Bioengineering*, **91**(2):169-179.
<http://dx.doi.org/10.1002/bit.20502>
- Kong, Q., Cheng, Y., Bao, X., et al., 2013. Solubility and partition coefficient of *p*-toluic acid in *p*-xylene and water. *Fluid Phase Equilibria*, **340**:46-51.
<http://dx.doi.org/10.1016/j.fluid.2012.12.009>
- Kumrić, K.R., Vladisavljević, G.T., Trtić-Petrović, T.M., 2012. Membrane-assisted liquid-phase extraction of Lu (III) in a U-shaped contactor with a single hollow fiber membrane. *Industrial & Engineering Chemistry Research*, **51**(43):14199-14208.
<http://dx.doi.org/10.1021/ie301887h>
- Li, X., Wang, L., Cheng, Y., et al., 2010. Water-saving Terephthalic Acid Production Method. CN Patent 201010241238.5 (in Chinese).
- Li, X.K., Ma, K.L., Meng, L.W., et al., 2014. Performance and microbial community profiles in an anaerobic reactor treating with simulated PTA wastewater: from mesophilic to thermophilic temperature. *Water Research*, **61**:57-66.

- <http://dx.doi.org/10.1016/j.watres.2014.04.033>
- Liu, W.F., Cheng, S.A., 2014. Microbial fuel cells for energy production from wastewaters: the way toward practical application. *Journal of Zhejiang University-SCIENCE A (Applied Physics & Engineering)*, **15**(11):841-861. <http://dx.doi.org/10.1631/jzus.A1400277>
- Lum, K.H., Cook, S.J., Stevens, G.W., et al., 2014. Zinc chloride and hydrochloric acid coextraction from galvanizing pickling waste in the presence of iron (II). Results with hollow fiber membrane contactors. *Industrial & Engineering Chemistry Research*, **53**(11):4453-4461. <http://dx.doi.org/10.1021/ie4036498>
- Macarie, H., Noyola, A., Guyot, J.P., 1992. Anaerobic treatment of a petrochemical wastewater from a terephthalic acid plant. *Water Science and Technology*, **25**(7):223-235.
- McCabe, W.L., Smith, J.C., Harriott, P., 1993. Unit Operations of Chemical Engineering. McGraw-Hill, New York, USA, p.658-683.
- Moreno, T., Tallon, S.J., Catchpole, O.J., 2014. Supercritical CO₂ extraction of 1-butanol and acetone from aqueous solutions using a hollow-fiber membrane contactor. *Chemical Engineering & Technology*, **37**(11):1861-1872. <http://dx.doi.org/10.1002/ceat.201300700>
- Nakao, F., Kamimura, Y., Murai, T., et al., 2006. Liquid-liquid Extraction Method. CN Patent 200610001441.9 (in Chinese).
- Pabby, A.K., Sastre, A.M., 2013. State-of-the-art review on hollow fibre contactor technology and membrane-based extraction processes. *Journal of Membrane Science*, **430**:263-303. <http://dx.doi.org/10.1016/j.memsci.2012.11.060>
- Ren, Z., Zhang, W., Dai, Y., et al., 2008. Modeling of effect of pH on mass transfer of copper (II) extraction by hollow fiber renewal liquid membrane. *Industrial & Engineering Chemistry Research*, **47**(12):4256-4262. <http://dx.doi.org/10.1021/ie0714798>
- Samaniego, H., San Román, M.F., Ortiz, I., 2007. Kinetics of zinc recovery from spent pickling effluents. *Industrial & Engineering Chemistry Research*, **46**(3):907-912. <http://dx.doi.org/10.1021/ie060836w>
- Shen, S., Smith, K., Cook, S., et al., 2009. Phenol recovery with tributyl phosphate in a hollow fiber membrane contactor: experimental and model analysis. *Separation and Purification Technology*, **69**(1):48-56. <http://dx.doi.org/10.1016/j.seppur.2009.06.024>
- Shirazian, S., Ashrafizadeh, S.N., 2011. Near-critical extraction of the fermentation products by membrane contactors: a mass transfer simulation. *Industrial & Engineering Chemistry Research*, **50**(4):2245-2253. <http://dx.doi.org/10.1021/ie101343r>
- Sun, J., 2014. Current technology and market analysis of PX and PTA. *China Chemical Trade*, **6**(17):58-60 (in Chinese).
- Thiruvenkatachari, R., Kwon, T.O., Jun, J.C., et al., 2007. Application of several advanced oxidation processes for the destruction of terephthalic acid (TPA). *Journal of Hazardous Materials*, **142**(1-2):308-314. <http://dx.doi.org/10.1016/j.jhazmat.2006.08.023>
- Vernekar, P.V., Jagdale, Y.D., Patwardhan, A.W., et al., 2013. Transport of cobalt (II) through a hollow fiber supported liquid membrane containing di-(2-ethylhexyl) phosphoric acid (D2EHPA) as the carrier. *Chemical Engineering Research and Design*, **91**(1):141-157. <http://dx.doi.org/10.1016/j.cherd.2012.06.019>
- Wang, H., Zhang, X., Huang, Z., et al., 2014. Simulation and design on extraction process for PTA wastewater. *Journal of Fuzhou University (Natural Science Edition)*, **42**(2):317-320 (in Chinese).
- Wickramasinghe, S.R., Semmens, M.J., Cussler, E.L., 1991. Better hollow fiber contactors. *Journal of Membrane Science*, **62**(3):371-388. [http://dx.doi.org/10.1016/0376-7388\(91\)80048-B](http://dx.doi.org/10.1016/0376-7388(91)80048-B)
- Wilke, C.R., Chang, P., 1955. Correlation of diffusion coefficients in dilute solutions. *AIChE Journal*, **1**(2):264-270. <http://dx.doi.org/10.1002/aic.690010222>
- Younas, M., Bocquet, S.D., Sanchez, J., 2008. Extraction of aroma compounds in a HFMC: dynamic modelling and simulation. *Journal of Membrane Science*, **323**(2):386-394. <http://dx.doi.org/10.1016/j.memsci.2008.06.045>
- Zhu, P.W., Dai, H., Han, L., et al., 2015. Aluminum extraction from coal ash by a two-step acid leaching method. *Journal of Zhejiang University-SCIENCE A (Applied Physics & Engineering)*, **16**(2):161-169. <http://dx.doi.org/10.1631/jzus.A1400195>

中文概要

题目: 对二甲苯非分散相溶剂萃取精对苯二甲酸工业废水中的对甲基苯甲酸

目的: 采用对二甲苯为萃取剂, 通过非分散相溶剂萃取(膜基萃取)同时回收利用精对苯二甲酸(PTA)工业废水中的对甲基苯甲酸和水。

创新点: 1. 采用非分散相溶剂萃取有效地实现了工业条件下 PTA 废水的净化和资源的回收利用; 2. 采用数学模拟优化工业萃取的操作参数。

方法: 1. 进行对二甲苯萃取实验, 考察操作条件对萃取效率和萃余水杂质浓度的影响; 2. 通过数学模拟, 建立膜萃取过程的数学模型, 对操作参数与膜结构参数进行敏感性分析。

结论: 1. 非分散相溶剂萃取可以有效解决 PTA 工业废水的回收利用问题; 2. 质量传递的速率控制步骤是管程中的水相扩散; 3. 优化的工业操作条件为: 中空纤维膜内径为 200~250 μm, 萃取时间为 50~60 s, 水油两相体积比为 9.0, 萃取温度为 318 K。

关键词: 非分散相溶剂萃取; PTA 废水; 对甲基苯甲酸; 对二甲苯; 质量传递